Pitch Dynamics Analysis for an Agricultural Tractor with Image Processing Validation through an Off-Board Camera

L. Onesto * **M. Corno** * **S. Savaresi** *

* *Dipartimento di Elettronica Informazione e Bioingegneria, Politecnico di Milano, via G. Ponzio 34/5, 20133, Milan, Italy. Email:* {*luca.onesto, matteo.corno, sergio.savaresi*}*@polimi.it.*

Abstract: This work proposes an analysis of the pitch dynamics of a heavy-duty vehicle, namely an agricultural tractor. Considering maneuvers performed on a flat-asphalt surface, the analysis is performed through an image processing approach. The analysis focuses on the cabin displacement and on the vehicle body displacement. Moreover, the tires compression and the vehicle longitudinal slip are evaluated. The analysis shows how the cabin and the body displacements change in function of the vehicle longitudinal acceleration and how, due to the tires compression, the cabin and the body can oscillate, at the end of a braking maneuver. The results are used to evaluate the feasibility of a road gradient estimator based on the inertial measurement of a mono axial accelerometer installed in the cabin. In particular, the cabin displacement needs to be considered and an additional sensor which measures the cabin speed is required to avoid a drop of performance.

Keywords: Vehicle dynamics, Pitch, Estimation Algorithms, Kalman Filters, Image Processing

1. INTRODUCTION

Modern Agricultural tractors are complex machines. They are designed to operate on a wide array of terrains and conditions. To better face these situations, they are equipped with complex hydraulic transmissions and suspension systems. Understanding the pitch dynamics of tractors in these varied conditions is useful to the design and tuning of many of the tractor subsystems: for example the cabin suspension control (see Langer et al. (2016)), traction control and automatic gear shifting (see Andersen et al. (2003)).

One of the most useful information on the tractor state is the road grade. The open scientific literature offers many examples of subsystems that employ the terrain grade information to improve the tractor performance and or safety. In Druzhinina et al. (2000) a braking system for a truck is developed, where the road gradient, estimated as a constant unknown parameter, is used to modulate the control action. Additionally, the knowledge of the road slope can be used to prevent needless shifting of automatic transmission. For this purpose, in Ohnishi et al. (2000) two estimation algorithms are developed for the case study of a car. One exploits the information of a longitudinal accelerometer, the others exploits the vehicle estimated torque. They conclude that with the inertial measurement the estimation is more accurate. The usage of torque and of inertial measurement is deeply compared in Lingman and Schmidtbauer (2002), focusing on heavy duty vehicles. For both approaches, an estimator is performed in a Kalman-filter fashion. Moreover, the estimation of the vehicle mass is also included. The estimation of the road slope is related to the longitudinal vehicle force. The inertial sensor provides a direct measurement of the longitudinal (specific) force. While, in the method based on the torque measurement, the force is obtained relying on a vehicle model. Hence, all the model uncertainties affects the results. For this reason, it is stated that the slope estimation accuracy increases when using an accelerometer.

In Corno et al. (2014) the usage of a reduced sensor set (i.e. longitudinal acceleration and speed) is used to develop a Kalman-filtering approach that considers the vehicle longitudinal dynamics, coupled with a fictitious road slope dynamics. The algorithm is developed for the case study of an Electrically Power Assisted Cycle.

This work focuses on the the vehicle pitch dynamics. The pitch dynamics analysis is performed through an image processing approach that allows the reconstruction of signals not available with the onboard sensors.

The pitch dynamics of a tractor are different from the ones of a car (that are well studied in the literature). In particular, a tractor differs from onroad vehicles under several aspects:

- The cabin and the vehicle body have a different pitch angle, because of the cabin suspension system.
- Many tractors are equipped with a front axles only load leveling suspension system.
- The tires of heavy-duty vehicles are subject to non negligible compressions in both vertical and longitudinal direction.
- Being off-highway vehicles, the tyres are subject to considerable longitudinal slip.

This paper is organized as follows. In Section 2, the experimental layout of the vehicle is presented. Section

3 presents and validates the image processing approach. Section 4 shows the experimental results of the pitch dynamics analysis. Finally, in Section 5, the results of the analysis are exploited to evaluate the feasibility of a road gradient estimator.

2. EXPERIMENTAL LAYOUT

The heavy-duty off-highway vehicle considered in this work consists in a tractor (model: Deutz-Fahr 6140). Figure 1 shows the elements that characterize the pitch dynamics of the tractor, namely: the cabin, the cabin suspension, the vehicle body, the front and the rear wheels, the front suspension. Note the tractor is not equipped with

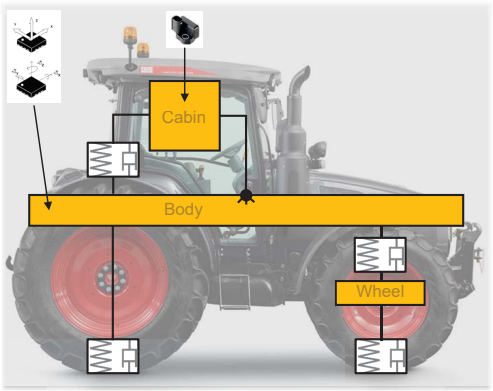

Fig. 1. Experimental layout

a rear suspension. The front suspension is pneumatic and a load-levelling control is in charge of keeping the suspension leveled. The load-levelling control consists of a quasi-static law and its response time is in the order of 5 seconds.

The vehicle is equipped with the following sensors:

- A mono axial accelerometer installed inside the cabin, that provides the longitudinal acceleration of the cabin A_{x_c}. This is the only accelerometer installed in the production vehicle.
- A 6 axis Inertial Measurement Unit (IMU) installed on the vehicle body. In the following analysis only the pitch rate $\dot{\theta}_B$ and the longitudinal acceleration A_{x_B} of the tractor body are considered. This IMU is installed only on the prototype and not on the production vehicle.
- An encoder installed in the transmission system, that provides the longitudinal speed V_{x_E} of the wheels. The encored is installed both on the prototype and on the production vehicle.

Moreover the vehicle is equipped with a cruise control system and a continuously variable transmission system. They allows the driver to set a reference speed to the tractor. In particular, this aspect will be exploited to perform speed inversion tests without acting on the brakes.

3. IMAGE ANALYSYS ALGORITHM

To perform the vehicle pitch dynamics, the cabin's pitch angle θ_C, the body's pitch angle θ_B, the longitudinal and the vertical compression of the front and rear wheels, Δ_{x_F}, Δ_{y_F}, Δ_{x_R} and Δ_{y_R} respectively, are considered. Please note that with the onboard sensors it is not possible to obtain all the mentioned variables, hence additional instrumentation is required. This can be avoided recording the maneuvers of the tractor through an external camera. In this Section, the image processing algorithm used to extract the informations from the videos is presented. Please note that with the proposed method it is possible to evaluate the longitudinal compression of the tires only when the wheels are locked.

The maneuvers are performed on the same flat-asphalt surface and registered by a camera (model: SONY RX100), fixed on a support, with a frame-rate of 250 frames per second. Figure 2 shows the experimental layout used for

Fig. 2. Experimental layout for image processing

the image analysis. Six markers (M_i, $i = 1,..,6$) are installed on the vehicle. Table 1 indicates for each marker, the supportive element, the height with respect to the road, when the vehicle is at standstill, and the depth with respect to the side of the tires. Analysing the position of the markers it is possible to measure the variables of interests.

The position of the marker in world coordinates is obtained following the steps:

(1) Lens distortion correction.
(2) Detection of the position of the markers on the image plane.
(3) Reprojection of the markers' position in world coordinates.

To accomplish the first and the third step of the procedure, the camera needs to be calibrated. According to the Pinhole Camera Model (see Heikkila and Silven (1997)), the relationship between the image plane and the world coordinates is:

$$[x\, y\, 1] = [X\, Y\, Z\, 1] \begin{bmatrix} R \\ t \end{bmatrix} K \tag{1}$$

where $[x\, y\, 1]$ are the coordinates in the image plane in pixel, $[X\, Y\, Z\, 1]$ are the world coordinates in meters, K is the intrinsic matrix (composed by the intrinsic parameters), while R and t are the Rotation matrix and the translation vector and compose the extrinsic parameters.

The world points are transformed to camera coordinates using the extrinsics parameters. The camera coordinates are mapped into the image plane using the intrinsics parameters.

In this work, the extrinsic and intrinsic parameters are obtained as discussed in Zhang (2000). In particular:

- the intrinsic parameters, describing the internal camera geometric and optical characteristics, are estimated using a training set of 80 pictures of a checkerboard pattern in different positions. The resulting reprojection error has a mean value of 0.3 pixel which is considered satisfactory for this application.
- the extrinsic parameters allow for the reprojection of the markers' position in world coordinates. Since the markers lay in five different (and parallel) vertical planes, five different sets of extrinsic parameters are defined. This is accomplished exploiting the information of the depth with respect to the tires side. Hence, for each marker the following translation vector t_i is defined:

$$t_i = \begin{bmatrix} t_x \\ t_y \\ t_z \end{bmatrix} + \begin{bmatrix} 0 \\ 0 \\ \delta_{z_i} \end{bmatrix}, \; i = 1, .., 6 \tag{2}$$

where t_x, t_y and t_z are the parameters of the translation vector, obtained from the camera calibration procedure. As regards the Rotation matrix R, since the five planes are parallel, it is the same for all the markers. The calibration procedure is performed placing a checkerboard on the side of the tires (see Figure 2). The resulting reprojection error has a mean value of 2.48 [mm].

Table 1. Markers configuration

Marker	**Element**	**Height [mm]**	$\delta_{\mathbf{z}}$ [mm]
M_1	Cabin	2715	655
M_2	Cabin	2700	525
M_3	Body	1110	1190
M_4	Body	1095	1190
M_5	Front Wheel	625	260
M_6	Body	825	335

As regards the second step of the procedure, for each frame, the position of the markers in the image plane is extracted through an Aggregate Channel Features (ACF) detector (see Dollár et al. (2014)). The detector, trained with 21 labelled images, provides the position (in pixels) of the candidate objects and their confidence score. Defining a threshold on the confidence score, it is possible to properly detect the location of the six markers within the image, as Figure 3 shows.

Once the markers' position in world coordinates are available, it is possible to measure the variables of interest as follows. The measurement of the cabin's pitch angle θ_C is obtained considering the line connecting M_1 and M_2. Defining (x_1, y_1) and (x_2, y_2) their position coordinates, the line linking M_1 M_2 can be expressed as:

$$y = m_{12} \cdot x + q \tag{3}$$

where its slope can be calculated as

$$m_{12} = \frac{y_1 - y_2}{x_1 - x_2} \tag{4}$$

Finally the cabin's pitch angle θ_C is obtained as

$$\theta_C = -\arctan(m_{12}) \tag{5}$$

Then, trough differentiation, it is possible calculate the cabin's pitch rate $\dot{\theta}_C$.

Fig. 3. Markers extraction trough ACF detector: on the top all the candidate objects, on the bottom only the markers selected checking the confidence scores

Following the same procedure, considering the pairs (M_3, M_4) and (M_3, M_6) it is possible to calculate the body's pitch rate $\dot{\theta}_B = \dot{\theta}_{34} = \dot{\theta}_{36}$.

Since the mentioned pairs are not aligned with respect to the vehicle's body, the body pitch angle θ_B can be computed as:

$$\begin{aligned} \theta_B &= \theta_{B_0} + \theta_{34} - \theta_{34_0} \\ &= \theta_{B_0} + \theta_{36} - \theta_{36_0} \end{aligned}$$

where θ_{B_0}, θ_{34_0} and θ_{36_0} are respectively the displacement of the body and of the two lines when the tractor is standing still.

The compression of the front and rear tires can be measured from the motion, in the longitudinal and in the vertical direction, of M_5 and M_6 respectively.

3.1 Validation of the Image Analysys Algorithm

Firstly, the performance of the camera calibration procedure are evaluated. From a random video frame, the position of the markers are manually obtained. Then, exploiting the intrinsic and the extrinsic parameters, the distance from the i-th and the j-th marker, called d_{ij} is measured and compared to the real one. The accuracy of the measurements is in the order of the centimeters. In particular the root mean square error is equal to 0.17 $[m]$.

The second phase of the validation is based on the velocity computation. It is possible to compare the velocity of the markers to directly measured values:

- the longitudinal speed V_{x_E} measured through a wheel encoder, and the longitudinal speed of the markers, which is obtained trough the differentiation of their longitudinal position, during a test without wheel slip.
- the body pitch rate $\dot{\theta}_B$ measured by the 6-axis IMU to the ones measured through video processing $\dot{\theta}_{34}$ and $\dot{\theta}_{36}$.

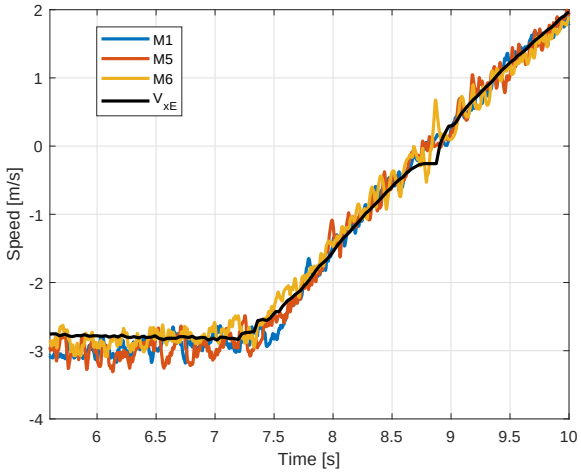

Fig. 4. Validation: speed comparison in a speed inversion test

Figure 4 shows the comparison of the longitudinal speed measured by the wheel encoder and by three markers, in a speed inversion test. The following remarks are due:

- The longitudinal speeds obtained from M_1, M_4 and M_5 are consistent with the one measured by the wheel encoder, however the Signal to Noise Ratio (SNR) is worse. In particular the root mean square error obtained considering all the six markers in the time window from 6 to 10 seconds is equal to 0.20 $\left[\frac{m}{s}\right]$.
- The wheels speed V_{x_E} is provided by an encoder. Hence, this measurement is not reliable around 0 $\left[\frac{m}{s}\right]$ (i.e. between 8.5 and 9 seconds).

Figure 5 shows the comparison of the body pitch rate measurements at the end of a braking maneuver. The following remarks are due:

- Both the measured pitch rate $\dot{\theta}_{34}$ and $\dot{\theta}_{36}$ are consistent with the one measured by the IMU. In particular, the root mean square error in the time window from 30 to 35 seconds is equal to 1.79 $\left[\frac{deg}{s}\right]$.
- Even in this case the image processing SNR is worse with respect to the one measured by the IMU.

Overall, the image processing tool provides a reliable, albeit noisy, method to measure the position and velocities of part of the tractor that cannot be directly measured with onboard sensors.

4. PITCH DYNAMICS ANALYSIS

The pitch dynamics of the tractor is analysed in the following case studies:

- Speed inversion
- Braking (to complete stop)

4.1 Speed inversion tests analysis

Figure 6 shows the pitch dynamics analysis of a speed inversion test. The following remarks are due:

- At the end of the acceleration transient the variation of the cabin displacement is around 2 degrees.

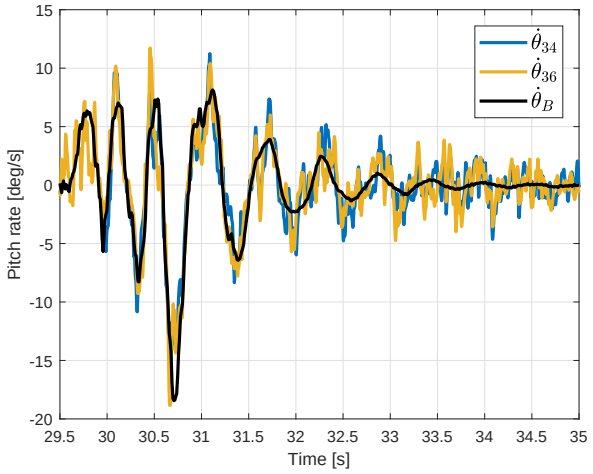

Fig. 5. Validation: pitch rate comparison at the end of an hard braking maneuver

- As regards the body displacement, at the end of the acceleration transient the vehicle body displacement increases by 1 degree. This fact is confirmed by the body pitch rate.

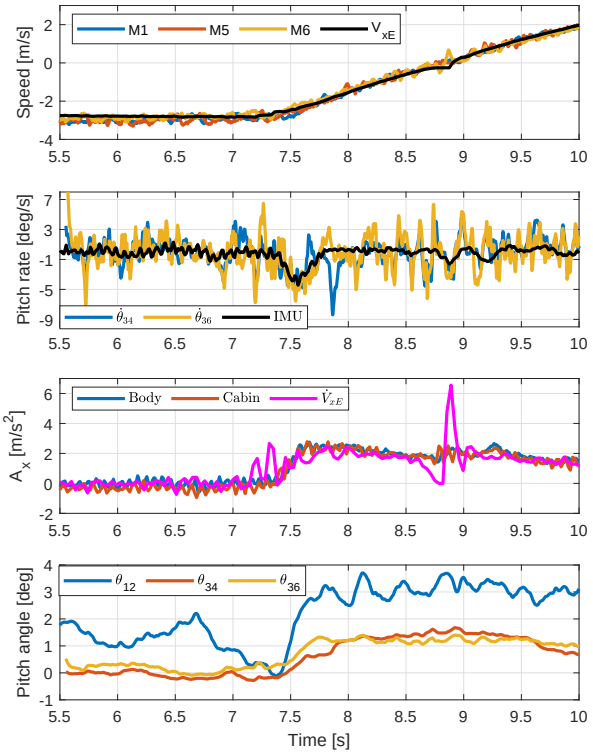

Fig. 6. Pitch dynamics analysis of a speed inversion test

4.2 Cabin and body displacement analysis through inertial measurements

The analysis of the body and of the cabin displacements can be performed using inertial measurements. The measurement of the accelerometer located in the cabin depends

on 3 factors: the road gradient θ, the vehicle's longitudinal acceleration $\dot{V}_x$ and the cabin displacement θ_C. The relationship is described by the following equation:

$$\dot{V}_x = A_{x_C} - g \cdot \sin(\theta + \theta_C)$$

In particular, the relationship between the vehicle's acceleration and the cabin displacement (i.e. $\theta_C = \theta_C(\dot{V}_x)$) is analysed. If the longitudinal slip is negligible, the vehicle's longitudinal acceleration can be obtained filtering the longitudinal wheels speed V_{x_E}. As regards the experimental tests:

- The tests are performed in plane, so the road gradient is zero. Hence, the cabin displacement can be analysed comparing the cabin acceleration A_{x_C} and the vehicle longitudinal acceleration.
- The cruise control is in charge to track the reference speed (respectively ± 5, ± 10 and ± 20 $\left[\frac{km}{h}\right]$) set by the driver. As showed in the following, the wheel slip effect can be neglected for this kind of tests.

Considering the vehicle body acceleration A_{x_B}, with the same procedure, it is possible to analyse the displacement of the vehicle body during the maneuvers. Figure 7 presents the comparison between the three accelerations. The following remarks are due:

- In first approximation, a linear relationship between the accelerations holds.
- The plot on the left shows how the cabin acceleration differs from the vehicle's one. This is due to the cabin displacement θ_C.
- The plot in the center shows that the body acceleration is almost the same of the vehicle's one, save for an offset. In other words, the vehicle body pitch dynamics is not perceptible from this analysis. This is may due to the measurement noise that characterizes both the measurements.
- The plot on the right shows that the body and the cabin accelerations are almost the same, except for an offset. This means that the body and the cabin displacements are different in absolute value, but they are subject to almost the same pitch angle variation.

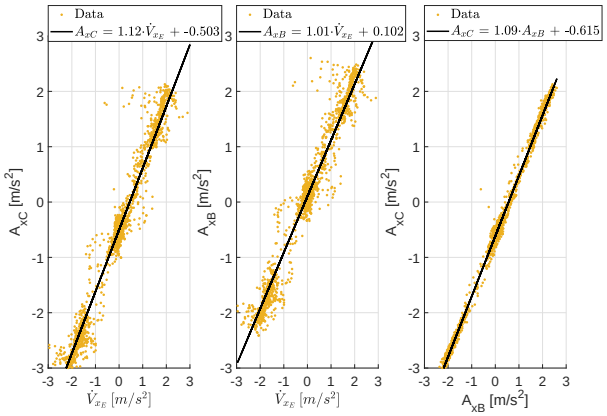

Fig. 7. Cabin and body displacement analysis performed through inertial measurements during speed inversion tests.

Overall, the analysis performed through the inertial measurements is consistent with the results obtained through the image processing approach. In particular, the cabin displacement θ_C affects the cabin acceleration A_{xC}.

4.3 Braking Maneuvers analysis

Figure 8 shows the pitch analysis of a braking maneuver test. The maneuver can be divided in two parts: the *Deceleration Phase* and the *Locked Wheel Phase*. The *Deceleration Phase* starts when the driver acts on the brakes and it ends when the wheels are locked. Then, the *Locked Wheel Phase* begins. During the *Deceleration Phase*:

- The difference between the wheels speed and the markers speed indicates the presence of slip.
- Figure 9 shows the wheel slip λ, calculated respect to the speed of M_5. In first approximation, it is possible to consider the wheel slip constant. In particular, the mean slip is $\bar{\lambda} = 0.25$ while the mean deceleration is $\bar{\dot{V}}_x = -6 \left[\frac{m}{s^2}\right]$.
- The image processing approach shows how the cabin and the vehicle body have a variation of displacement of -2 and -1 degrees respectively.
- At the beginning of the braking maneuver, the front and the rear tire has a compression of +3 and -3 centimeters. This fact is due to the load transfer.

During the *Locked Wheel Phase*:

- At the beginning of the phase, both the wheels and the markers speeds are zero. This means that the vehicle does not go forward anymore when the wheels are locked. However the vehicle body and the cabin are affected by oscillation. This is due to the tires compression.
- In particular, the front and the rear tires have a longitudinal compression of 5 centimeters. Hence, even if the wheels are locked, the cabin and the vehicle body are subject to accelerations.
- The body and the cabin oscillations last for 3 seconds circa.

5. FINAL CONSIDERATIONS ON TERRAIN GRADE ESTIMATION

This Section discusses the feasibility of a road gradient estimator based on the longitudinal accelerometer installed inside the cabin. The considered approach is the one presented in Corno et al. (2014), where the developed algorithm is based on the vehicles longitudinal dynamics:

$$\dot{V}_x = A_{x_M} - g \cdot \sin(\theta) \tag{6}$$

where A_{x_M} is the measured longitudinal acceleration, g is the gravitational acceleration in $\left[\frac{m}{s^2}\right]$, $\dot{V}_x$ is the time derivative of the vehicle's longitudinal speed and θ is the road slope. Defining the variable $\theta^\star$ as:

$$\theta^\star = \sin(\theta)$$

the model becomes linear. Including a fictitious road slope dynamics, (6) can be rewritten in state space form:

$$\begin{cases} \dot{V}_x = A_{x_M} - g \cdot \theta^\star + \eta_{x1} \\ \dot{\theta}^\star = \eta_{x2} \\ y = V_x + \eta_y \end{cases}$$

where η_{x1}, η_{x2} and η_y are Gaussian noises. A Kalman filter can be designed to estimate the state variables of the

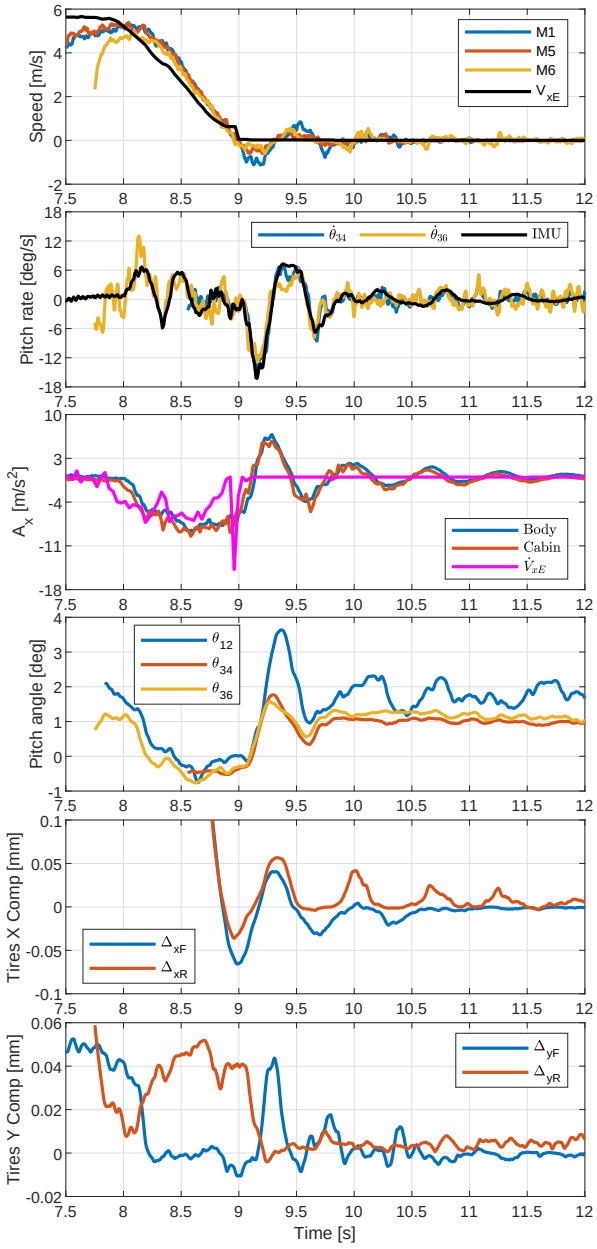

Fig. 8. Pitch dynamics analysis of a braking test

system, namely V_x and $\theta^\star$. The inputs of the algorithm are the measurements of the longitudinal speed V_{x_E} and of the longitudinal acceleration A_{x_C}. Then, the following consideration can be done:

- As shown in Subsection 4.2, the cabin displacement θ_C affects the cabin acceleration A_{x_C}. Hence, a compensation of the cabin displacement is required to preserve the estimation performances.
- Due to the wheel slip λ, defined as $\lambda = \frac{V_x - V_{x_E}}{V_x}$, the real speed of the vehicle V_x is not available. Since it is not computable from the available signals, it is not possible to compensate its effect. However, in low slip conditions, the estimation performance of the proposed approach is satisfactory. If the wheel slip is not negligible, an additional sensor providing the cabin speed is required to avoid a drop of performance.

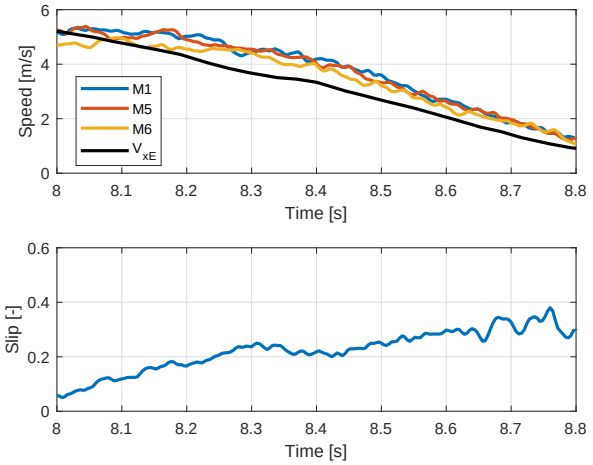

Fig. 9. Experimental results: slip during the Deceleration phase

REFERENCES

Andersen, T.O., Hansen, M.R., and Conrad, F. (2003). Robust control of oscillations in agricultural tractors. In *ASME 2003 International Mechanical Engineering Congress and Exposition*, 89–95. American Society of Mechanical Engineers.

Corno, M., Spagnol, P., and Savaresi, S.M. (2014). Road slope estimation in bicycles without torque measurements. *IFAC Proceedings Volumes*, 47(3), 6295–6300.

Dollár, P., Appel, R., Belongie, S., and Perona, P. (2014). Fast feature pyramids for object detection. *IEEE Transactions on Pattern Analysis and Machine Intelligence*, 36(8), 1532–1545.

Druzhinina, M., Moklegaard, L., and Stefanopoulou, A. (2000). Compression braking control for heavy-duty vehicles. In *American Control Conference, 2000. Proceedings of the 2000*, volume 4, 2543–2547. IEEE.

Heikkila, J. and Silven, O. (1997). A four-step camera calibration procedure with implicit image correction. In *Computer Vision and Pattern Recognition, 1997. Proceedings., 1997 IEEE Computer Society Conference on*, 1106–1112. IEEE.

Langer, T., Holm-Petersen, K., and Metker, D. (2016). Comfort evaluation criteria for pitching vibration damping of agricultural tractors. *74th Internationale Tagung Landtechnik (Agricultural Engineering), VDI Berichte*, (2273), 437–44.

Lingman, P. and Schmidtbauer, B. (2002). Road slope and vehicle mass estimation using kalman filtering. *Vehicle System Dynamics*, 37(sup1), 12–23.

Ohnishi, H., Ishii, J., Kayano, M., and Katayama, H. (2000). A study on road slope estimation for automatic transmission control. *JSAE review*, 21(2), 235–240.

Zhang, Z. (2000). A flexible new technique for camera calibration. *IEEE Transactions on pattern analysis and machine intelligence*, 22.